ADVANCED MATERIALS
www.advmat.de

Photochromic Control in Hybrid Perovskite Photovoltaics

*Weifan Luo, José María Andrés Castán, Diego Mirani, Antonio J. Riquelme, Amit Kumar Sachan, Olzhas Kurman, SunJu Kim, Fabiola Faini, Paul Zimmermann, Alexander Hinderhofer, Yash Patel, Aaron T. Frei, Jacques-E. Moser, Daniel Ramirez, Frank Schreiber, Pascale Maldivi, Ji-Youn Seo, Wolfgang Tress, Giulia Grancini, Renaud Demadrille, and Jovana V. Milić**

The application of perovskite photovoltaics is hampered by issues related to the operational stability upon exposure to external stimuli, such as voltage bias and light. The dynamic control of the properties of perovskite materials in response to light could ensure the durability of perovskite solar cells, which is especially critical at the interface with charge-extraction layers. We have applied a functionalized photochromic material based on spiro-indoline naphthoxazine at the interface with hole-transport layers in the corresponding perovskite solar cells with the aim of stabilizing them in response to voltage bias and light. We demonstrate photoinduced transformation by a combination of techniques, including transient absorption spectroscopy and Kelvin probe force microscopy. As a result, the application of the photochromic derivative offers improvements in photovoltaic performance and operational stability, highlighting the potential of dynamic photochromic strategies in perovskite photovoltaics.

1. Introduction

Hybrid organic-inorganic metal halide perovskite materials have become a promising alternative to conventional semiconductors in next-generation solar cells.[1] They are based on the AMX_3 perovskite structure defined by the central A cation (typically methylammonium (MA^+), formamidinium (FA^+), or Cs^+) with divalent metal (M) such as Pb^{2+}, occupying the octahedral cage, and halide ions (typically I^- or Br^-) situated at the corners (**Figure 1a**).[2] They have exceptional optoelectronic properties; however, ensuring long-term stability remains a major challenge for practical applications.[3] Several factors influence the stability of perovskite solar cells, such as the susceptibility

W. Luo, Y. Patel, J. V. Milić
Adolphe Merkle Institute/ University of Fribourg
Fribourg 1700, Switzerland
E-mail: jovana.milic@unifr.ch

J. M. A. Castán, D. Mirani, A. J. Riquelme, P. Maldivi, R. Demadrille
Université Grenoble Alpes
CEA
CNRS
Grenoble-INP, IRIG-SyMMES, 17 avenue des Martyrs, Grenoble 38000, France

A. K. Sachan, W. Tress
Forschungsschwerpunkt Organic Electronics & Photovoltaics
ZHAW School of Engineering
Winterthur 8400, Switzerland

O. Kurman, S. Kim, J.-Y. Seo
Department of Nanoenergy Engineering
Pusan National University
Busan 46241, South Korea

F. Faini, G. Grancini
Physical Chemistry Department
University of Pavia
Pavia 27100, Italy

P. Zimmermann, A. Hinderhofer, F. Schreiber
Institute of Applied Physics
University of Tübingen
72076 Tübingen, Germany

A. T. Frei, J.-E. Moser
Photochemical Dynamic Group
Institute of Chemical Sciences and Engineering
École Polytechnique Fédérale de Lausanne
Lausanne 1015, Switzerland

D. Ramirez
Centro de Investigación
Innovación y Desarrollo de Materiales – CIDEMAT
Facultad de Ingeniería
Universidad de Antioquia UdeA
Calle 67 No. 52-21, Medellín 050010, Colombia

J. V. Milić
Department of Chemistry
University of Turku
Turku 20500, Finland

The ORCID identification number(s) for the author(s) of this article can be found under https://doi.org/10.1002/adma.202420143

DOI: 10.1002/adma.202420143

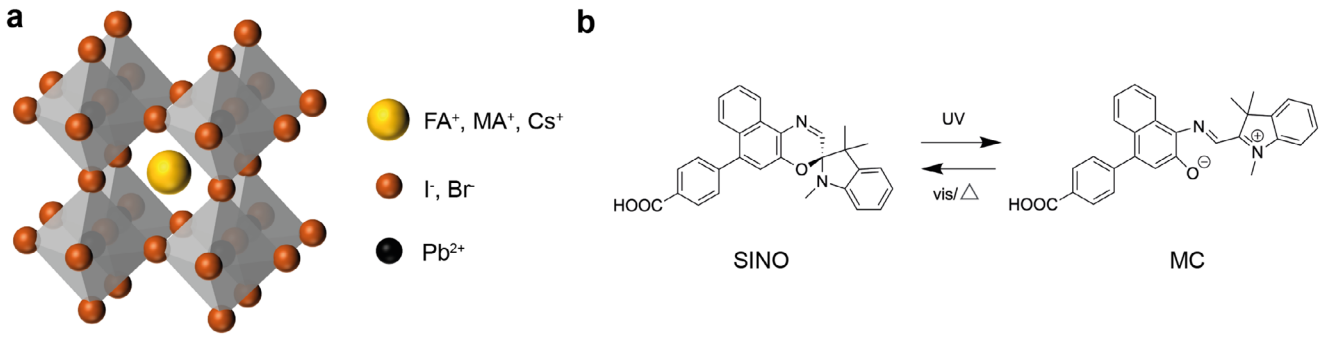

Figure 1. Photochromic halide perovskite modulation. Schematic of (a) hybrid metal halide perovskite (AMX_3) structure, with characteristic components, and (b) SINO photoswitch, reversibly transforming from the closed into open merocyanine (MC) form upon UV irradiation.

to ion migration accelerated under operating conditions of temperature fluctuation, voltage bias, and light.[4] Control of these factors is required to achieve competitive efficiency and long-term operational stability in photovoltaics. Various strategies have been used to address the inherent instability,[5] such as relying on hydrophobic organic moieties at the perovskite interface.[6] While these approaches have contributed to improvements in stability, they lack the ability to adapt to external stimuli, such as light, despite the potential to address the dynamic changes that occur during device operation.[7]

To enable the material to respond dynamically to changes during operation, photochromic systems capable of undergoing photoinduced transformation are especially relevant, changing their properties when exposed to light.[8] In particular, spiro-indoline naphthopyrans are a class of photochromic compounds endowed with desirable attributes suitable for various applications, including sensing, ion detection, and optical lenses.[9–11] In perovskite solar cells, a common approach to enhance performance involves using functional organic cations at the interface, reducing non-radiative recombination of charge carriers.[4–6] However, this method lacks dynamic adaptability, as the material cannot respond to changes in the environment. Despite the extensive exploration of photochromic materials, only a few have been investigated within the realm of photovoltaics, and the integration of these systems into perovskite-based solar cells remains underexploited. In 2015, a bis-thienylethene derivative was first introduced into dye-sensitized solar cells.[12–14] Subsequently, certain diarylethenes (DAEs) were utilized in photochromic organic solar cell devices.[14] However, the photoisomer interconversion in such molecules could only be achieved through successive ultraviolet (UV) and visible (vis) light irradiation cycles.[15] Similarly, spiropyran and the corresponding spirobenzo and naphthoxazine families were also evaluated in dye-sensitized solar cells yet their switching within the devices was not realized under device operating conditions.[11] Moreover, the bistability of DAEs prevents their dynamic adaptability under solar cell operation conditions.[16] In addition, limited fatigue resistance in the solid state presents a significant impediment to incorporating photochromic compounds into photovoltaics.[17] Hence, most of the photochromic materials have only been studied in solution.[17] In this respect, the soft yet crystalline structure of halide perovskites[18] holds promise for their application in perovskite optoelectronics, which remains to be exploited.[19]

Here, we employed a photochromic material, 4-(1,3,3-trimethylspiro[indoline-2,3′-naphtho[2,1-b][1,4]oxazin]-6′-yl)benzoic acid (SINO) at the interface with the perovskite layer in perovskite solar cells. We applied various characterization techniques, such as transient absorption spectroscopy and Kelvin probe force microscopy (KPFM), complemented with theoretical calculations, to assess the interactions at the interface, as well as photochromic behavior in the solid state. The interfacial changes resulted in improved photovoltaic performance and operational stability, validated through day-night cycling, demonstrating the potential of photochromic materials.

2. Results and Discussion

2.1. Molecular Design

Spiro-indoline naphthoxazine core was functionalized for incorporation into perovskite-based photovoltaic devices by introducing a carboxyl group to enable its binding to the perovskite surface via hydrogen bonding and metal coordination (Figure 1b). The SINO derivative converts to the merocyanine (MC) form upon irradiation which can be thermally reversed (Figure 1b).[9] This allows for photoinduced switching between the closed SINO and the open MC form featuring a larger dipole moment relevant for ion binding and suppressing ion migration while facilitating charge extraction at the interface. Conversely, in the dark cyclization of the original spiro form would facilitate reversible ion migration which would not interfere with the perovskite recovery. This can be enabled by the corresponding SINO energy levels of its highest occupied (HOMO) and lowest unoccupied molecular orbitals (LUMO),[9] which are appropriately aligned for charge extraction at the hole-transport layer when SINO adopts its open conformation as indicated by theoretical calculations.[11] Accordingly, using SINO derivatives in perovskite devices could help improve their operational stability without compromising photovoltaic device performance.

2.2. Photochromic Characteristics in Solution and The Solid-State

To evaluate the concept and understand the hybrid material, the SINO derivative was synthesized following the adaptation of

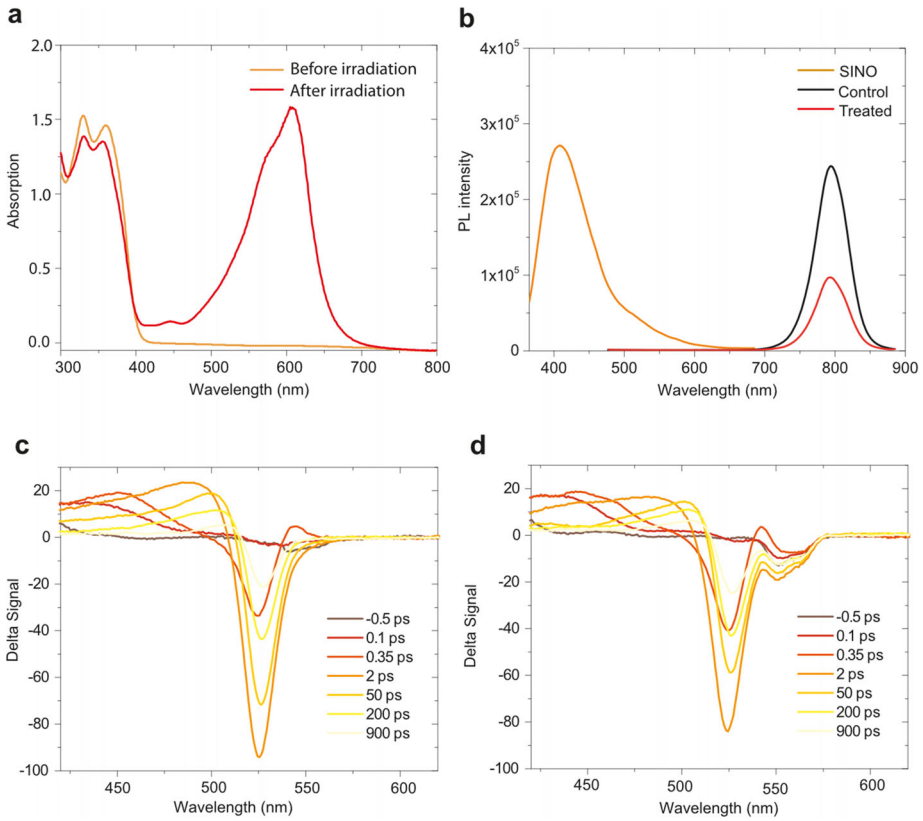

Figure 2. Photochromism in solution and the solid state. (a) UV–vis absorption spectra of SINO (0.1 mM in toluene) at ambient temperature before and after irradiation by a 200–600 nm (200 W) xenon lamp. The MC form is apparent through the emergence of a signal at around 600 nm, which is more pronounced for higher-power xenon (200 W) lamps than LED (ca. 500 mW) irradiation. (b) Steady-state PL of the control (triple-cation) and SINO-treated perovskite films. (c) Transient absorption spectra of pristine $MAPbBr_3$ (control) and treated (d) with SINO overlayers. TAS spectra of the $Cs_{0.05}FA_{0.90}MA_{0.05}Pb(I_{0.95}Br_{0.05})_3$ perovskite films are shown in Figures S4 and S5 of the Supporting Information. Although the time constants for the underlying processes are not precisely known, it can be assumed that interfacial charge transfer (ps) is much faster than the molecular photoswitch (s).

previously reported procedures, as detailed in the Experimental Section of the Supporting Information.[9] Its photochromic behavior was initially studied in the solution of tetrahydrofuran (THF) or toluene, which are orthogonal solvents for perovskite thin films. Upon irradiating the solution (0.1 mM) with a xenon lamp (200–600 nm, 200 W), UV-vis spectra reveal the emergence of the absorption around 600 nm, associated with the MC form (**Figure** 2a). The original spectra recovered upon light source removal, suggesting reversible photochromism.[9]

Having confirmed the photoswitching of SINO in solution, we investigated its photochromism in the solid state. We deposited a solution of SINO in toluene (0.5 mg/mL) onto a conventional triple-cation perovskite of $Cs_{0.05}FA_{0.90}MA_{0.05}Pb(I_{0.95}Br_{0.05})_3$ composition and monitored the X-ray diffraction patterns of the films in ambient air (Figure S1). From the diffraction patterns, we observe that the films consist of the α-phase perovskite and the degradation product, PbI_2.[20] With the exposure to air, the amount of PbI_2 increases substantially in the control sample, while the amount in the SINO-treated sample remains much lower, suggesting that the SINO acted as a protective layer, suppressing phase degradation. X-ray photoemission spectroscopy (XPS) measurements further evidenced the SINO overlayer on the perovskite surface (Figure S2). Specifically, the SINO-treated 3D perovskite films exhibited an additional N 1*s* signal, whereas the Pb 4*f* and I 3*d* signals shifted to a lower energy region, and the C 1*s* signal shifted to a higher binding energy. These shifts indicate that SINO interacts with metal cations and halide anions of the perovskite at the surface.[21] To further assess the impact on the surface properties of perovskite, we conducted the grazing incidence wide-angle X-ray scattering (GIWAXS) measurements on SINO-treated perovskite films (Figure S3). The control film exhibited characteristic diffraction rings indicative of the 3D perovskite structure.[20] While a crystalline phase of SINO could not be observed under these experimental conditions (Figure S3), films with SINO featured substantially less hexagonal phase (δ-phase) than the control sample, validating a stabilizing role. However, the orientation of the perovskite did not change with the addition of SINO, excluding bulk structural changes. We thus employed in-situ GIWAXS upon irradiation to assess the photochromic response at the interface (Figure S3). We analyzed the diffraction patterns of the SINO-treated samples before and after a 15-min irradiation with 365 nm LED lamp. The photoswitch did not result in observable structural changes in the perovskite material under these conditions suggesting that the changes in the photoswitch do not induce structural transformations in the perovskite layer.

The interfacial photoswitching was thereby assessed by monitoring the optical properties of SINO at the interface.

Steady-state photoluminescence (PL) spectra (Figure 2b) of the films upon depositing SINO solution revealed PL quenching in the SINO-treated samples upon excitation at 350 nm from the front and back (glass) side.[22] To assess the underlying charge carrier dynamics, we relied on transient absorption spectroscopy (TAS) of perovskite films treated with SINO (Figure S4 and S5 and Figure 2c,d). We monitored the dynamic evolution of photoexcited species upon photoexcitation above the band gap of the triple-cation perovskite (Figure S4 and S5). The rate constants for the thermal back reaction have been previously estimated in solution, and bleaching was found to take seconds.[9] The precise estimate depends on the polarity of the medium and steric hindrance,[9] which are challenging to estimate in the solid state; yet, it is reasonable to assume that the rates for both forward and backward photoreactions are slower than in the solid state due to steric hindrance and that they are much slower than the interfacial charge transfer processes. The absorbance (A) of SINO-treated perovskite for the excitation pump wavelength of 350 nm was 1.3. Considering the thickness (t) of the perovskite layer from cross-sectional scanning electron microscopy (SEM) analysis (Figure S6) of approximately 500 nm, a laser penetration depth (d) in the material ($d = 1/\alpha = t/A$, where α is the absorption coefficient) can be estimated at 385 nm. The thickness of the SINO overlayer is not expected to exceed 20 nm based on the concentration of the solution. Therefore, the 350 nm excitation wavelength used for PL measurements can be assumed to penetrate the bulk reaching nearly the perovskite/SINO interface capable of effectively triggering the photoswitch and nonradiative processes through interactions with the perovskite, leading to PL quenching. We retrieved the differential absorption (DA) signal as a function of pump-probe delay and monitored the ground state photobleaching (PB) evolution of the band edge transition at 785 nm. We used a pump wavelength (λ_{pump}) of 500 nm and 380 nm to enable the photoswitch of SINO selectively. With $\lambda_{pump} = 500$ nm, we only excited the triple-cation perovskite, without the photoswitch. The comparison of the PB dynamics in the control and the treated sample showed a prolonged decay in the SINO-treated samples, indicating the passivation effect upon interaction with the perovskite surface.[22–25] This also suggests that SINO acts as a protective layer,[26,27] corroborating XRD results. Furthermore, upon the photoswitch of the SINO ($\lambda_{pump} = 380$ nm), we observed a progressive rise in the PB. Since the absorption of the MC form overlaps with the spectral characteristics of the triple cation perovskite materials. We also monitored the TA spectra of $MAPbBr_3$ (Figure 2c–d) due to its distinct optoelectronic properties that feature minimal spectral overlap with SINO, facilitating the identification of optical signals.[23] The XPS analysis confirmed the interaction with the perovskite through the changes in the Pb 4*f* characteristic peaks for the $MAPbBr_3$ before and after UV exposure (Figure S7).[24] In the TAS experiments, $MAPbBr_3$ perovskite films were excited at 400 nm and the resulting spectra (Figure 2d) showed two distinct features that is a prominent PB centered around 520 nm, attributed to the $MAPbBr_3$ perovskite phase,[25] and a negative signal at approximately 550 nm corresponding to the absorption of the MC form of SINO,[9] in accordance with the expected photoinduced conversion.

Such photochromism of SINO in the solid state was also expected to alter the surface potential at the perovskite interface, further assessed by high-resolution frequency-modulated Kelvin probe force microscopy (FM-KPFM). This allowed us to investigate the contact potential difference (V_{CPD}) between the gold-coated AFM probe and the sample surface with high spatial and temporal resolution. The AFM height profile indicated that the surface morphology remains unchanged with SINO (Figure S8). While control perovskite films (i.e., triple cation perovskite on FTO glass) exhibited an average V_{CPD} value of -75 mV (**Figure 3**a), the perovskite films coated with a thin layer of SINO showed an average V_{CPD} of around 0 mV (Figure 3a). The V_{CPD} maps for each film also displayed two cycles of UV light exposure (marked dark areas in Figure 3b). In-situ V_{CPD} mapping of the control perovskite film demonstrated a V_{CPD} shift of approximately -50 mV under UV exposure, while the target perovskite film exhibited a shift of approximately −120 mV (Figure 3b). This indicates the photoswitch caused a V_{CPD} shift of about −70 mV in the SINO-coated film. Notably, the V_{CPD} of the SINO-coated surface fully recovered to its initial value instantly after turning off the UV light,[28] indicating the reversibility of the photoswitching process.

The difference in the surface potential can be associated with the changes in the dipole moment of SINO, which was also investigated theoretically (Figure 3c,d; Figure S9, and Table S1, Supporting Information). Density functional theory (DFT) calculations suggest a different binding mode of the SINO to the interface of hybrid perovskite in the closed and the open (MC) form, as well as a distinct binding to other interfaces, such as metal oxide surfaces, as in glass substrates or charge-transport layers. For instance, at the interface with the TiO_2, SINO undergoes deprotonation of the carboxylate group via oxygenated basic sites at the surface of TiO_2[29] resulting in a strong affinity for Ti^{4+} without significantly altering the energetics between the forms compared to the isolated molecule (Figure 3d). The dipole moments of SINO in both forms remain comparable to those of isolated molecules. In contrast, when SINO interacts with the perovskite, the carboxylic function cannot be deprotonated and shows a weaker affinity for Pb^{2+} indicating a preference for hydrogen bonding with FA and halide ions instead through weak electrostatic and van der Waals interactions (Figure 3c). As a result, the dipole moment varies significantly between the open and closed forms of SINO, corroborating the findings of the KPFM and XPS measurements. Moreover, the interaction affects the formation energies of the MC form, facilitating the photoswitching at the perovskite interface (as detailed in the Supporting Information). The photoswitch is further facilitated by the soft yet crystalline structure of the metal halide perovskites and the orientation of SINO at the interface. Such photochromism at the surface is expected to affect photovoltaics.

2.3. Photovoltaic Characteristics

The impact of a SINO layer on the photovoltaic performance was investigated in conventional n-i-p perovskite solar cells with an architecture of fluorine-doped tin oxide (FTO)/c-TiO_2/mp-TiO_2/perovskite/2,2′,7,7′-tetrakis[*N*,*N*-di(4-methoxyphenyl)amino]-9,9′-spirobifluorene (Spiro-OMeTAD)/Au (**Figure 4**a). The performance was evaluated by measuring the current-voltage (J–V) characteristics under a AM 1.5 light source (Figure 4b). Incorporating SINO as an

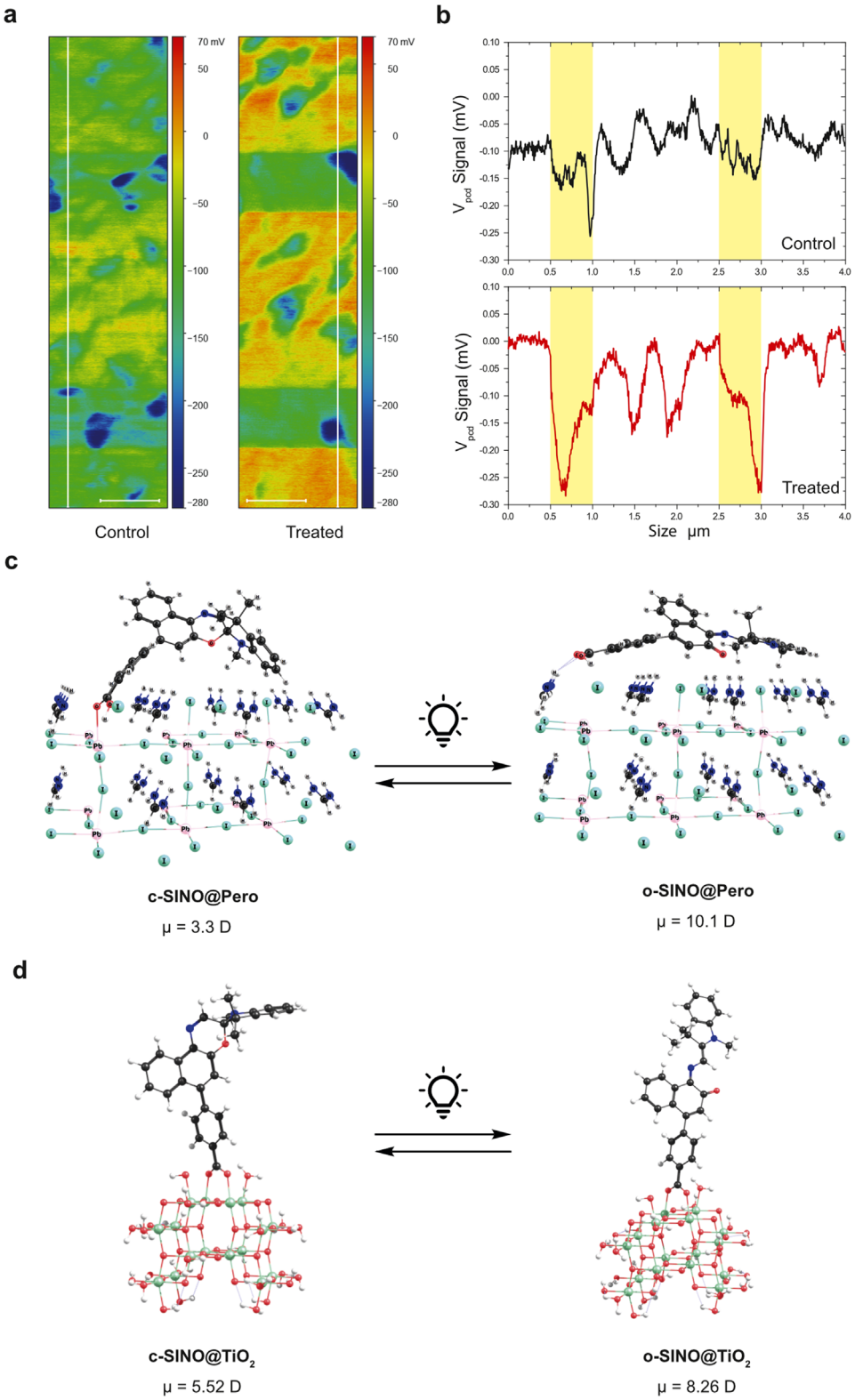

Figure 3. Photochromism in the solid state. (a) KPFM V_{CPD} signal maps and (b) V_{CPD} signal profile of the control (mixed cation) perovskite and control samples treated with SINO (irradiation periods and sections are highlighted in yellow). (c–d) Structural representation of the binding of SINO (c-SINO, left) and its open (o-SINO, MC) form (right) on the surface of (c) the perovskite framework (SINO@Pero) and (d) TiO_2 substrate (SINO@TiO_2) with the corresponding dipole moments µ based on DFT calculations.

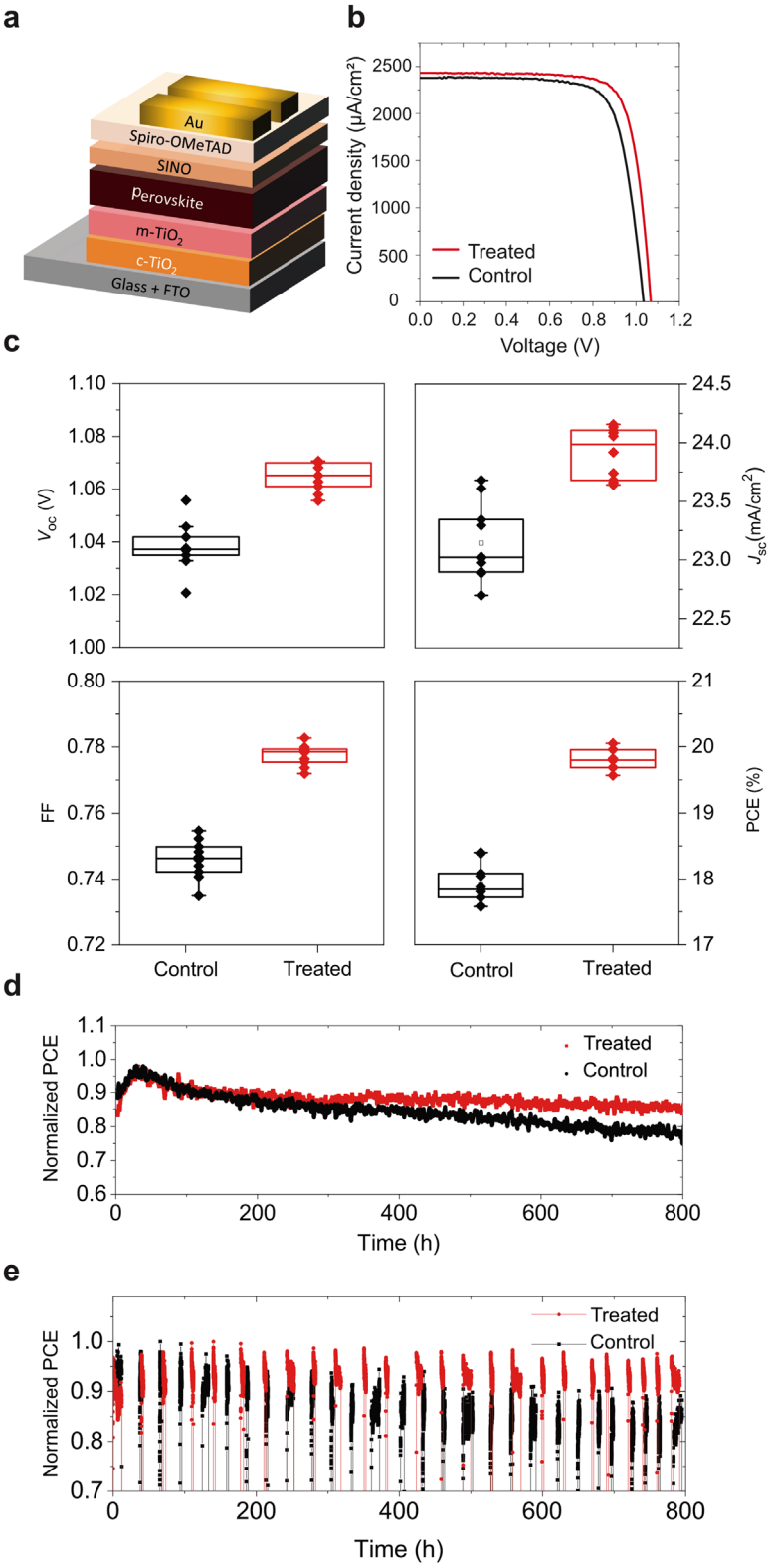

Figure 4. Photovoltaic performance in photochromic perovskite solar cells. (a) Schematic of the n-i-p solar cell (using $Cs_{0.05}FA_{0.90}MA_{0.05}Pb(I_{0.95}Br_{0.05})_3$. (b) *J–V* curves of the champion control and SINO-treated devices under AM 1.5G illumination. (c) Statistical distribution of open-circuit voltage (V_{OC}), short-circuit current density (J_{SC}), fill factor (FF), and power conversion efficiency (PCE) for 16 devices. (d) Continuous MPP tracking of control and SINO-treated solar cells in a nitrogen atmosphere under one sun irradiation at ambient temperature and (e) evolution of the PCE during day-night simulated operation.

overlayer on the perovskite resulted in higher open-circuit voltage (V_{OC}) and fill factor (FF), with minor short-circuit current (J_{SC}) improvements, and consequently, improved power conversion efficiency (PCE). The incident photon-to-current efficiency (IPCE) spectra excluded significant spectral mismatch (Figure S10a). The champion devices exhibited PCEs over 20% (Figure 4c), which can be further optimized to match the performances of the state-of-the-art devices in the future beyond the scope of this work. For the generality of the approach, we also investigated the impact on wide bandgap $MAPbBr_3$ devices, which showed comparable performance improvements (Figure S10b). The improvements in the open circuit voltage for triple cation perovskite devices corroborated the passivation effect of the SINO, which was in accordance with the time-resolved photoluminescence spectroscopy (TRPL; Figure S11) and transient absorption spectroscopy (Figure 2c,d) analysis.

The impact on the charge-carrier extraction was further assessed by ultraviolet photoelectron spectroscopy (UPS; Figure S12–S13) and electrochemical impedance spectroscopy (EIS, Figures S14–S16). UPS spectra showed reduced ionization energy (IE) upon applying SINO compared to the control perovskite, which was the result of surface interactions and a higher dipole moment. This also resulted in increased work function (WF) upon UV irradiation,[30,31] corroborating KPFM and PL measurements (Figure S11), as well as photovoltaic performance, likely due to reduced energy barriers for hole injection.[32,33] Moreover, XPS spectra change upon UV irradiation (Figure S7). The change in the control samples results from the generation of free charge carriers, the stimulation of ion migration, and the formation of interfacial defects that can collectively affect binding energies. Upon SINO treatment, the magnitude of these changes is reduced, which is likely due to UV absorption[19,34] and the contribution to suppressing some of the interfacial changes. The underlying factors governing solar cell performance were investigated by electronic impedance spectroscopy (EIS; Figure S15 and S16) using a protocol established for photochromic dye-sensitized solar cells.[34] It was assumed that applying SINO at the perovskite interface could result in suppressed ion migration, reflected in the reduced hysteresis of SINO-containing solar cells. Accordingly, the forward and reverse *J-V* scans at varying rates (0.01–1 V/s) provided the degree of hysteresis (DoH) estimate using the following equation.[35]

$$\mathrm{DoH} = 100\frac{A_{\mathrm{rev}} - A_{\mathrm{for}}}{Max.\left(A_{\mathrm{rev}}.A_{\mathrm{for}}\right)}\% \quad (1)$$

A reduction in DoH was observed for cells incorporating SINO at either interface (Figure S14), which can be attributed to reduced ion migration, which is relevant to performance and stability.[36] In addition, the photoactivation of SINO molecules on top of the perovskite film resulted in the negative values of DoH, which can be linked to modifications in the potential at the interface.[35]

The EIS spectra of perovskite solar cells display two semicircles, one at high frequencies, primarily associated with geometrical capacitance and electronic recombination, and another at low frequencies, largely influenced by ionic properties (Figure S15).[37] The introduction of SINO led to a more pronounced low-frequency signal, which indicates an effective interfacial modulation of ionic migration, enhancing its response to voltage perturbation. This was accompanied by the decrease in the height of the low-frequency signals when SINO was applied at the interface below the perovskite layer, which can be explained by a reduction in mobile ion vacancy density.[38] The two semicircle spectra were fit using an equivalent circuit consisting of two RC elements in series to each other to elucidate the recombination and ionic properties of the devices. Although the recombination lifetime for cells with SINO under the perovskite layer was shorter than that of the control, this was likely due to the changes in geometrical capacitance, as the recombination resistances did not show enough differences to justify this change in time constant (Figure S15 and S16, Table S2). Specifically, the presence of dipoles at the interface may alter the dielectric constant or the roughness factor of the devices[39] which can modify geometrical capacitance.[40] To assess the impact of this interfacial change on the charge collection efficiency (CCE), a comparison of the impedance at the V_{OC} and 0 V under illumination was used to estimate the CCE (Figure S17, Table S3).[41] For this purpose, we compared the CCE for devices containing SINO at the interface with either electron- (TiO_2) or hole-transport (spiro-OMeTAD) layers. While most devices featured CCE above 90%, indicating that SINO does not impede charge extraction, this was not the case for devices containing SINO at the interface with the electron-transport layer. This suggests electronic transport issues, such as interfacial energetics or ionic accumulation, revealing a more effective use at the hole-transport layer interfaces, which can be explained by differences in the formation of Debye layer close to the ETL or HTL, accelerating or hindering charge extraction, respectively (as depicted in Figure S17).

The interfacial changes were expected to affect operational stability. We assessed the operational stability by monitoring the maximum power point (MPP) of n-i-p devices under continuous one-sun irradiation in a nitrogen atmosphere at ambient temperature. In the continuous stress test, SINO-treated devices demonstrated an advantage over the control ones, degrading by only about 15% after 800 h, unlike the control devices that lost over 20% of their performance (Figure 4d). To simulate real-world conditions, the devices were subjected to cycles of LED irradiation at 12h intervals. After 800 h of testing, the MPP retention exceeded 90% for the SINO-treated samples, compared to 80% for the control ones (Figure 4e), demonstrating the beneficial effects of the photochromic system under conditions simulating real-world operation.[42,43] While other systems have been studied under real-world operation[42–45] to our knowledge, this has not involved any dynamic materials and interfaces designed to adapt to such operating conditions. Moreover, photoactive spiroxazine systems were recently found relevant to enhancing resistance to UV irradiation,[19] which can stimulate further investigation of photochromic systems. This underscores the potential of photochromism in perovskite solar cells, providing a strategy for dynamically controlling materials during operation, which remains to be exploited.

3. Conclusion

In summary, we have demonstrated the proof-of-concept for the dynamic control of spiro-indoline naphthoxazine (SINO) at the perovskite interface. The photochromic properties of the SINO

switch were characterized using UV-vis, PL, and transient absorption spectroscopy. In addition, XRD showed that SINO can serve as a protective layer to suppress degradation. Kelvin probe force microscopy revealed reversible surface potential changes under irradiation, signifying photochromism in the solid state, while its effect on interfacial ion migration was verified by impedance spectroscopy. SINO was applied to perovskite solar cells, demonstrating improved power conversion efficiency, associated with defect passivation and improved contacts with the hole-transport layer, which can be further optimized in the future. Finally, this improved operational stability resulted in only 15% and 10% degradation upon continuous irradiation and 12-hour cycling, respectively, after 800 h. This illustrates the potential for photochromic control under real-world operating conditions, opening new perspectives for dynamic photochromic materials in photovoltaics.

Supporting Information

Supporting Information is available from the Wiley Online Library or from the author.

Acknowledgements

Weifan Luo and Jovana V. Milić acknowledge funding from the Swiss National Science Foundation project no. 193174, and the fellowship from the Swiss Leading House for the Latin American Region for support. They also appreciate the generous support of Prof. Ullrich Steiner and Dr. Efrain Ochoa-Martinez (Adolphe Merkle Institute, University of Fribourg) throughout the project. Jovana V. Milić, Renaud Demadrille, José María Andrés Castán, and Antonio J. Riquelme, Diego Mirani and Pascale Maldivi, Amit Kumar Sachan, and Tress Wolfgang acknowledge the European Research Council (ERC) for funding. We acknowledge the ESRF project no. 98610 and 93090 for the provision of synchrotron facilities and we would like to thank Dimitry Chernyshov and Vadim Dyadkin for assistance in using beamline BM01 and Lena Merten for measuring the GIWAXS. Alexander Hinderhofer thanks the BMBF for funding project ErUM-pro no. 05K19VTA. This work was funded under the European Union's Horizon 2020 research and innovation programme (grant agreement number 832606; project PISCO; 851676, project OptEIon). We appreciate the support of Agata in the design of the table of content figure and the associated video.

Open access publishing facilitated by Universite de Fribourg, as part of the Wiley - Universite de Fribourg agreement via the Consortium Of Swiss Academic Libraries.

Conflict of Interest

The authors declare no conflict of interest.

Author Contributions

W. L., J. M. A. C., and D. M. contributed equally to this work. The project was conceptualized by Jovana V. Milić and led by Weifan Luo, who conducted the characterization of the thin films and the fabrication of the solar cell devices with the support of Yash Patel. The SINO photoswitch was synthesized and characterized by José María Andrés Castán and Diego Mirani under the supervision of Renaud Demadrille, whereas Antonio J. Riquelme performed impedance spectroscopy. Amit Kumar Sachan conducted the KPFM measurements, whereas Amit Kumar Sachan and Tress Wolfgang analyzed the KPFM data. The TAS measurements were performed by Aaron T. Frei and Fabiola Faini under the supervision of Jacques-E. Moser and Giulia Grancini, respectively. GIWAXS measurements were performed by Paul Zimmermann and Alexander Hinderhofer with the support of Frank Schreiber, whereas Olzhas Kurman and SunJu Kim conducted UPS, PL, TRPL, and IPCE measurements, as well as complementary device fabrication and characterization, under the supervision of Ji-Youn Seo. Daniel Ramirez supported the complementary analysis of perovskite solar cells and stability assessment under real-world operating conditions. Pascale Maldivi performed theoretical calculations. All authors contributed to the manuscript and discussion.

Data Availability Statement

Data presented here can be accessed at the following https://doi.org/10.5281/zenodo.14876810, and it is available under the license CC-BY-4.0 (Creative Commons Attribution-ShareAlike 4.0 International).

Keywords

metal halide perovskites, perovskite solar cells, photochromic materials, photoswitch

Received: December 20, 2024
Revised: February 10, 2025
Published online: March 20, 2025

[1] J. P. Correa-Baena, M. Saliba, T. Buonassisi, M. Grätzel, A. Abate, W. Tress, A. Hagfeldt, *Science* **2017**, *358*, 739.
[2] A. K. Jena, A. Kulkarni, T. Miyasaka, *Chem. Rev.* **2019**, *119*, 3036.
[3] Y. G. Rong, Y. Hu, A. Y. Mei, H. R. Tan, M. I. Saidaminov, S. I. Seok, M. D. McGehee, E. H. Sargent, H. W. Han, *Science* **2018**, *361*, eaat8235.
[4] R. Wang, M. Mujahid, Y. Duan, Z. K. Wang, J. J. Xue, Y. Yang, *Adv. Funct. Mater.* **2019**, *29*, 1808843.
[5] H. W. Zhu, S. Teale, M. N. Lintangpradipto, S. Mahesh, B. Chen, M. D. McGehee, E. H. Sargent, O. M. Bakr, *Nat. Rev. Mater.* **2023**, *8*, 569.
[6] J. Kim, A. Ho-Baillie, S. J. Huang, *Sol. RRL* **2019**, *3*, 1800302.
[7] K. Domanski, B. Roose, T. Matsui, M. Saliba, S. H. Turren-Cruz, J. P. Correa-Baena, C. Roldán-Carmona, G. Richardson, J. M. Foster, F. De Angelis, J. M. Ball, A. Petrozza, N. Mine, M. K. Nazeeruddin, W. Tress, M. Grätzel, U. Steiner, A. Hagfeldt, A. Abate, *Energy Environ. Sci.* **2017**, *10*, 604.
[8] R. Pardo, M. Zayat, D. Levy, *Chem. Soc. Rev.* **2011**, *40*, 672.
[9] J. M. A. Castán, V. M. Mwalukuku, A. J. Riquelme, J. Liotier, Q. Huaulmé, J. A. Anta, P. Maldivi, R. Demadrille, *Mater. Chem. Front.* **2022**, *6*, 2994.
[10] G. Such, R. A. Evans, L. H. Yee, T. P. Davis, *J. Macromol. Sci. Polym. Rev.* **2003**, *C43*, 547.
[11] V. Barachevsky, *Rev. J. Chem.* **2013**, *3*, 52.
[12] S. Ma, H. Ting, Y. Ma, L. Zheng, M. Zhang, L. Xiao, Z. Chen, *AIP Adv.* **2015**, *5*, 057154.
[13] M. J. Noah, Y. S. Yuriy, S. Chris, H. Daniel, S. Masoud, K. S. L. Kenneth, J. Hai-Feng, *AIMS Mater. Sci.* **2015**, *2*, 503.
[14] B. W. Saes, M. M. Wienk, R. A. Janssen, *RSC Adv.* **2020**, *10*, 30176.
[15] W. J. Wu, J. X. Wang, Z. W. Zheng, Y. Hu, J. Y. Jin, Q. Zhang, J. L. Hua, *Sci. Rep.* **2015**, *5*, 8592.
[16] Y. Wang, H. Yang, K. Zhang, M. Q. Tao, M. Z. Li, Y. L. Song, *ACS Energy. Lett.* **2022**, *7*, 3646.
[17] A. Gonzalez, E. S. Kengmana, M. V. Fonseca, G. G. D. Han, *Mater. Today Adv.* **2020**, *6*, 100058.
[18] L. A. Muscarella, A. Ducinskas, M. Dankl, M. Andrzejewski, N. P. M. Casati, U. Rothlisberger, J. Maier, M. Graetzel, B. Ehrler, J. V. Milic, *Adv. Mater.* **2022**, *34*, 2108720.

[19] T. Zhou, W. Zhao, Z. Wang, R. Li, X. Feng, Y. Du, L. Liu, J. Zhang, G. Yin, K. Wang, H. Yu, Y. Liu, Q. Tian, S. (Frank) Liu, *Adv. Energy Mater.* **2024**, 2404850.
[20] L. Q. Xie, L. Chen, Z. A. Nan, H. X. Lin, T. Wang, D. P. Zhan, J. W. Yan, B. W. Mao, Z. Q. Tian, *J. Am. Chem. Soc.* **2017**, *139*, 3320.
[21] I. S. Zhidkov, D. W. Boukhvalov, A. F. Akbulatov, L. A. Frolova, L. D. Finkelstein, A. I. Kukharenko, S. O. Cholakh, C. C. Chueh, P. A. Troshin, E. Z. Kurmaev, *Nano Energy* **2021**, *79*, 105421.
[22] D. W. deQuilettes, S. M. Vorpahl, S. D. Stranks, H. Nagaoka, G. E. Eperon, M. E. Ziffer, H. J. Snaith, D. S. Ginger, *Science* **2015**, *348*, 683.
[23] L. C. Chen, J. R. Wu, Z. L. Tseng, C. C. Chen, S. H. Chang, J. K. Huang, K. L. Lee, H. M. Cheng, *Materials* **2016**, *9*, 747.
[24] S. Tan, T. Huang, I. Yavuz, R. Wang, M. Weber, Y. Zhao, M. Abdelsamie, M. Liao, H.-C. Wang, K. Huynh, K.-H. Wei, J. Xue, F. Babbe, M. Goorsky, J.-W. Lee, C. Sutter-Fella, Y. Yang, *J. Am. Chem. Soc.* **2021**, *143*, 6781.
[25] C. S. Ponseca, T. J. Savenije, M. Abdellah, K. B. Zheng, A. Yartsev, T. Pascher, T. Harlang, P. Chabera, T. Pullerits, A. Stepanov, J. P. Wolf, V. Sundström, *J. Am. Chem. Soc.* **2014**, *136*, 5189.
[26] S. Cacovich, D. Messou, A. Bercegol, S. Bechu, A. Yaiche, H. Shafique, J. Rousset, P. Schulz, M. Bouttemy, L. Lombez, *ACS Appl. Mater. Interfaces* **2020**, *12*, 34784.
[27] L. Calió, S. Kazim, M. Grätzel, S. Ahmad, *Angew. Chem., Int. Ed.* **2016**, *55*, 14522.
[28] Z. G. Xiao, Y. B. Yuan, Y. C. Shao, Q. Wang, Q. F. Dong, C. Bi, P. Sharma, A. Gruverman, J. S. Huang, *Nat. Mater.* **2015**, *14*, 193.
[29] P. Chen, J. H. Yum, F. D. Angelis, E. Mosconi, S. Fantacci, S.-J. Moon, R. H. Baker, J. Ko, M. K. Nazeeruddin, M. Grätzel, *Nano Lett.* **2009**, *9*, 2487.
[30] T. Yang, Zuo, Y., *Mater. Des.* **2021**, *207*, 109867.
[31] Catalán, J., *Phys. Chem. Chem. Phys.* **2015**, *17*, 12515.
[32] Petrović, M., Maksudov, T., Panagiotopoulos, A., Serpetzoglou, E., Konidakis, I., Stylianakis, M. M., Stratakis, E., Kymakis, E., *Nanoscale Adv* **2019**, *1*, 3107.
[33] Cheng, J., Xie, F., Liu, Y., Wei, S., Li, X., Yang, Y., W. C. Choy, *J. Mater. Chem. A* **2015**, *3*, 23955.
[34] A. J. Riquelme, V. M. Mwalukuku, P. Sánchez-Fernández, J. Liotier, R. Escalante, G. Oskam, R. Demadrille, J. A. Anta, *ACS Appl. Energy. Mater.* **2021**, *4*, 8941.
[35] N. E. Courtier, J. M. Cave, J. M. Foster, A. B. Walker, G. Richardson, *Energy Environ. Sci.* **2019**, *12*, 396.
[36] G. Richardson, S. E. J. O'Kane, R. G. Niemann, T. A. Peltola, J. M. Foster, P. J. Cameron, A. B. Walker, *Energy Environ. Sci.* **2016**, *9*, 1476.
[37] E. Von Hauff, D. Klotz, *J. Mater. Chem. C.* **2022**, *10*, 742.
[38] A. Riquelme, L. J. Bennett, N. E. Courtier, M. J. Wolf, L. Contreras-Bernal, A. B. Walker, G. Richardson, J. A. Anta, *Nanoscale* **2020**, *12*, 17385.
[39] A. Pockett, G. E. Eperon, N. Sakai, H. J. Snaith, L. M. Peter, P. J. Cameron, *Phys. Chem. Chem. Phys.* **2017**, *19*, 5959.
[40] A. Pockett, G. E. Eperon, T. Peltola, H. J. Snaith, A. Walker, L. M. Peter, P. J. Cameron, *Phys. Chem. Chem. Phys.* **2015**, *119*, 3456.
[41] I. Zarazúa, S. Sidhik, T. Lopéz-Luke, D. Esparza, E. De la Rosa, J. Reyes-Gomez, I. Mora-Seró, G. Garcia-Belmonte, *J. Phys. Chem. Lett.* **2017**, *8*, 6073.
[42] W. Tress, K. Domanski, B. Carlsen, A. Agarwalla, E. A. Alharbi, M. Graetzel, A. Hagfeldt, *Nat. Energy* **2019**, *4*, 568.
[43] M. Wu, N. Haji Ladi, Z. Yi, H. Li, Y. Shen, M. Wang, *Energy Techn* **2020**, *8*, 1900744.
[44] M. V. Khenkin, E. A. Katz, A. Abate, G. Bardizza, J. J. Berry, C. Brabec, F. Brunetti, V. Bulović, Q. Burlingame, A. Di Carlo, R. Cheacharoen, Y.-B. Cheng, A. Colsmann, S. Cros, K. Domanski, M. Dusza, C. J. Fell, S. R. Forrest, Y. Galagan, D. Di Girolamo, M. Grätzel, A. Hagfeldt, E. Hauff, H. Hoppe, J. Kettle, H. Köbler, M. S. Leite, S. F. Liu, Y.-L. Loo, J. M. Luther, et al., *Nat. Energy* **2020**, *5*, 35.
[45] D. Ramirez, J. V. Milić, *Mater. Today Electron.* **2023**, *4*, 100038.